Anticancer Activity and Cisplatin Binding Ability of *Bis*-Quinoline and *Bis*-Isoquinoline Derived [Pd$_2$L$_4$]$^{4+}$ Metallosupramolecular Cages

Roan A. S. Vasdev [1,2,3]*, Lachlan F. Gaudin [1], Dan Preston [1], Jackmil P. Jogy [3], Gregory I. Giles [3] and James D. Crowley [1,2]*

[1] Department of Chemistry, University of Otago, Dunedin, New Zealand, [2] MacDiarmid Institute for Advanced Materials and Nanotechnology, Wellington, New Zealand, [3] Department of Pharmacology and Toxicology, University of Otago, Dunedin, New Zealand

New *bis*-quinoline (**L$_q$**) and *bis*-isoquinoline-based (**L$_{iq}$**) ligands have been synthesized, along with their respective homoleptic [Pd$_2$(**L$_q$** or **L$_{iq}$**)$_4$]$^{4+}$ cages (**C$_q$** and **C$_{iq}$**). The ligands and cages were characterized by ^{1}H, ^{13}C and diffusion ordered (DOSY) NMR spectroscopies, high resolution electrospray ionization mass spectrometry (HR-ESIMS) and in the case of the *bis*-quinoline cage, X-ray crystallography. The crystal structure of the **C$_q$** architecture showed that the [Pd$_2$(**L$_q$**)$_4$]$^{4+}$ cage formed a twisted *meso* isomer where the [Pd(**quinoline**)$_4$]$^{2+}$ units at either end of the cage architecture adopt the opposite twists (left and right handed). Conversely, Density Functional Theory (DFT) calculations on the **C$_{iq}$** cage architecture indicated that a lantern shaped conformation, similar to what has been observed before for related [Pd$_2$(**L$_{tripy}$**)$_4$]$^{4+}$ systems (where **L$_{tripy}$** = 2,6-*bis*(pyridin-3-ylethynyl)pyridine), was generated. The different cage conformations manifest different properties for the isomeric cages. The **C$_{iq}$** cage is able to bind, weakly in acetonitrile, the anticancer drug cisplatin whereas the **C$_q$** architecture shows no interaction with the guest under the same conditions. The kinetic robustness of the two cages in the presence of Cl$^-$ nucleophiles was also different. The **C$_{iq}$** cage was completely decomposed into free **L$_{iq}$** and [Pd(Cl)$_4$]$^{2-}$ within 1 h. However, the **C$_q$** cage was more long lived and was only fully decomposed after 7 h. The new ligands (**L$_{iq}$** and **L$_q$**) and the Pd(II) cage architectures (**C$_{iq}$** and **C$_q$**) were assessed for their cytotoxic properties against two cancerous cell lines (A549 lung cancer and MDA-MB-231 breast cancer) and one non-cancerous cell line (HDFa skin cells). It was found that **L$_q$** and **C$_q$** were both reasonably cytotoxic (IC$_{50S}$ ≈ 0.5 μM) against A549, while **C$_{iq}$** was slightly less active (IC$_{50}$ = 7.4 μM). **L$_{iq}$** was not soluble enough to allow the IC$_{50}$ to be determined against either of the two cancerous cell lines. However, none of the molecules showed any selectivity for the cancer cells, as they were all found to have similar cytotoxicities against HDFa skin cells (IC$_{50}$ values ranged from 2.6 to 3.0 μM).

Keywords: palladium(II), anticancer, self-assembly, metallosupramolecular, quinoline

INTRODUCTION

Metallosupramolecular architectures (MSAs) (Cook and Stang, 2015) have been attracting increasing attention over the past two decades due to their many potential applications including catalysis (Yoshizawa et al., 2009; Yoshizawa and Fujita, 2010; Martí-Centelles et al., 2018), storage (Mal et al., 2009), and sensing (Wang et al., 2011). Inspired by the success of cisplatin and other metallodrugs (Mjos and Orvig, 2014) there is emerging interest in exploiting MSAs for biomedical purposes (Cook et al., 2013; Therrien, 2015; Casini et al., 2017; Zhou et al., 2017). Several groups have examined MSAs as drug delivery vectors (Therrien et al., 2008; Schmitt et al., 2012; Yi et al., 2012; Zheng et al., 2015; Samanta et al., 2016, 2017; Bhat et al., 2017; Xu et al., 2017; Wang J.-F. et al., 2018; Yue et al., 2018). Additionally, MSAs have been shown to bind DNA (Oleksy et al., 2006; Garci et al., 2017; Zhao et al., 2017) and RNA (Phongtongpasuk et al., 2013; Malina et al., 2015), interact with proteins (Li et al., 2014; Mitchell et al., 2017) and have anticancer (Hotze et al., 2008; Faulkner et al., 2014; Grishagin et al., 2014; Dubey et al., 2015; Zheng et al., 2016; Allison et al., 2018) and antibacterial (Richards et al., 2009; Howson et al., 2012; Wang H. et al., 2018) properties.

Since the pioneering work of McMorran and Steel (McMorran and Steel, 1998) interest in [M2(L)4]$^{n+}$ cage-type structures has burgeoned (Schmidt et al., 2014). Some time ago now we reported that a [Pd2(L$_{tripy}$)4]$^{4+}$ cage (where L$_{tripy}$ = 2,6-bis(pyridin-3-ylethynyl)pyridine) could host two molecules of the anticancer drug cisplatin within the cavity of the cage (Lewis et al., 2012), and thus had potential as a drug delivery vector. Disappointingly, the binding event, which was governed mainly by hydrogen bonding interactions, was weak (Preston et al., 2015). The host-guest complex formed in acetonitrile (CH$_3$CN) and dimethylformamide (DMF) but unfortunately in more hydrogen bond competitive solvents such as water and dimethyl sulfoxide (DMSO) no host-guest interaction was observed. Additionally, the parent Pd(II) based cage decomposed rapidly in the presence of nucleophiles (Lewis et al., 2012; McNeill et al., 2015). Thus, in order to exploit these [Pd2(L)4]$^{4+}$ cages as cisplatin delivery vehicles these issues need to be addressed. We and others have examined a range of modifications to the parent [Pd2(L)4]$^{4+}$ cage system in order to improve the solubility (Lewis and Crowley, 2014; Preston et al., 2015; Han et al., 2017) and other properties (Lewis et al., 2013, 2014; Kaiser et al., 2016; Schmidt et al., 2016a) of the cage. Efforts have also been made to enhance the strength of the host-guest interaction (Kim et al., 2015) and the stability of the cages in the presence of biologically revelant nucleophiles (Preston et al., 2016). However, while some improvements have been made these [Pd2(L)4]$^{4+}$ cages still require further modifcations in order to be useful drug delivery vectors.

The [Pd2(L)4]$^{4+}$ cages have also been examined for their cytotoxic properties. We showed that the parent [Pd2(L$_{tripy}$)4]$^{4+}$ was modestly cytotoxic (IC$_{50}$ values range from 40 to 70 μM) against a range of cancer cell lines but was less active than related bis-1,2,3-triazole [Pd2(L)4]$^{4+}$ helicates (McNeill et al., 2015). We also examined the cytotoxicity of related amino substituted [Pd2(L)4]$^{4+}$ cages against the same panel of cancer cells and found that they exhibited similar cytotoxic properties as the

parent systems (Preston et al., 2016). Casini, Kühn and co-workers (Kaiser et al., 2016; Schmidt et al., 2016b) have measured the cytotoxicity of a series of related [Pd2(L)4]$^{4+}$ cages and observed similar IC$_{50}$ values (10–70 μM). Additionally, they have measured the cytotoxicity of mixtures of the cages and cisplatin and unsurprisingly have found that those mixtures are more cytotoxic than cage alone (IC$_{50}$ = 2–13 μM). Yoshizawa, Ahmedova and co-workers have also found that [M2(L)4]$^{4+}$ (M = Pd^{2+} or Pt^{2+}) cages with similar, but more hydrophobic, dipyridyl anthracenyl ligands (L$_{anthracene}$) display high anticancer activity (IC$_{50}$ values range from 0.9 to 37.4 μM against HL-60, HL-60/Dox, HT-29, T-24, SKW-3 cancer cell lines) (Ahmedova et al., 2016; Anife et al., 2016).

The majority of the [Pd2(L)4]$^{4+}$ cages examined to date feature pyridyl donors, as part of our efforts to improve the biological properties of these systems herein we describe the use of isoquinoline and quinoline-derived ligands for the assembly of two new [Pd2(L)4]$^{4+}$ cages. While is well-known that isoquinoline and quinoline ligands can bind with palladium(II) and platinum(II) (Bondy et al., 2004) their use as donor systems in ligands for the generation MSAs has not been extensively explored (Bloch et al., 2016, 2017). These quinoline derived systems feature different electronic and steric properties compared to the parent pyridyl systems thus we also examine the effect these changes have on the host-guest chemistry with cisplatin, the stability of the cages in the presence of nucleophiles and the antiproliferative properties of the cages.

RESULTS AND DISCUSSION

The synthesis of the new quinoline (L$_q$) and isoquinoline (L$_{iq}$) based ligands was facile (**Supplementary Material**). Using sequential Sonogashira carbon-carbon cross coupling reactions from commercially available building blocks the ligands were generated in good yields (L$_q$ = 86% and L$_{iq}$ = 78%). ^{1}H and ^{13}C NMR spectroscopic data were consistent with the formation of the ligands which was supported by high-resolution electrospray mass spectrometry (HR-ESIMS) (**Figure 1** and **Supplementary Material**). Peaks corresponding to protonated and sodiated ligand were observed at m/z = 382.1320 and 404.1132, respectively, for L$_{iq}$ and similar peaks were observed for L$_q$ (**Supplementary Material**).

With the ligands in hand, the complexation with [Pd(CH$_3$CN)4](BF$_4$)2 in acetonitrile was examined (**Figure 1**). The cage formation was monitored using ^{1}H NMR spectroscopy (CD$_3$CN, 298 K) and showed that mixing [Pd(CH$_3$CN)4](BF$_4$)2 and the L$_{iq}$ ligand at room temperature (RT) in a 1:2 ratio led to the rapid (<2 min) and quantitative formation of the expected C$_{iq}$ cage (**Figure 1**), similar to what was observed with the parent L$_{tripy}$ system (Lewis et al., 2012). Interestingly, the behavior of L$_q$ with [Pd(CH$_3$CN)4](BF$_4$)2 at room temperature was very different. After 5 min at RT the reaction mixture displayed multiple proton resonances, none of which were due to free ligand, consistent with the formation of a mixture of different cage isomers. The reaction was monitored using ^{1}H NMR spectroscopy for 24 h at RT however little to no changes were
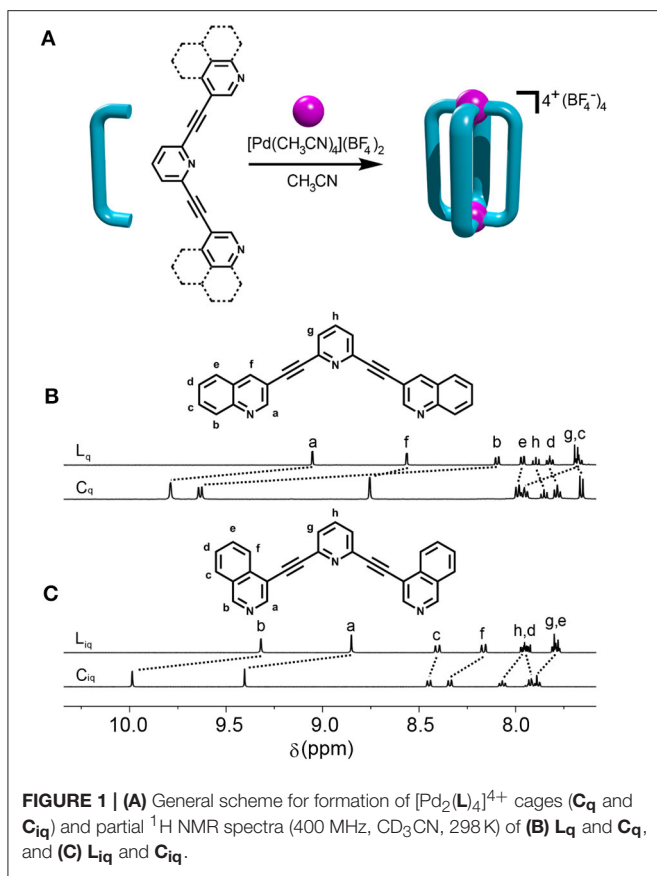
FIGURE 1 | **(A)** General scheme for formation of [Pd$_2$(**L**)$_4$]$^{4+}$ cages (**C$_q$** and **C$_{iq}$**) and partial ^{1}H NMR spectra (400 MHz, CD$_3$CN, 298 K) of **(B) L$_q$** and **C$_q$**, and **(C) L$_{iq}$** and **C$_{iq}$**.

observed after the first hour and the spectrum still displayed multiple proton resonances. A ^{1}H DOSY experiment (CD$_3$CN, 298 K) on the mixture showed that all the different proton resonances had the same diffusion co-efficient consistent with the postulate that the reaction mixture contains a series of cage isomers (**Supplementary Material**).

The assembly reaction between **L$_q$** with [Pd(CH$_3$CN)$_4$](BF$_4$)$_2$ was then carried out at 65°C, in CD$_3$CN and again monitored using ^{1}H NMR spectroscopy (**Figure 2**). After 5 min the same complicated series of proton resonance were observed. However, with continued heating this slowly resolved into a single series of resonances (after 7 h), consistent with the formation of a single cage isomer (**Figure 2**). Pleasingly, both cages (**C$_{iq}$** and **C$_q$**) could be isolated by adding diethyl ether into the acetonitrile reaction mixtures providing the cages as colorless/tan precipitates in 88% (**C$_{iq}$**) or 92% (**C$_q$**) yield, respectively. ^{1}H NMR spectroscopy (CD$_3$CN, 298 K) exhibited the expected downfield shifts of the signals pertaining to protons H$_a$, H$_b$ and H$_f$ as well as the anticipated downfield shifts of the rest of the isoquinoline and quinoline protons resonances (**Figure 1**). HR-ESIMS data also supported the formation of the cages, showing ions corresponding to the loss of 2, 3 and 4 tetrafluoroborate (BF$_4^-$) counterions (m/z = 956.1610 (2$^+$), 608.4424 (3$^+$), and 434.5832 (4$^+$), **Supplementary Material**). ^{1}H DOSY experiments (CD$_3$CN, 298 K) on the ligands (Diffusion coefficients (D) = 13.1 (**L$_q$**) and 15.0 (**L$_{iq}$**) x 10^{-10} m^2 s^{-1}) and

cages (D = 4.1 (**C$_q$**) and 4.3 (**C$_{iq}$**) × 10^{-10} m^2 s^{-1}) were also consistent with the formation of the larger [Pd$_2$(**L**)$_4$]$^{4+}$ cages (**Supplementary Material**).

Crystals of **C$_q$** suitable for X-ray diffraction formed during the cooling of an acetonitrile solution of the cage from 65°C to room temperature. The structure was solved in the tetragonal space group P4/*mnc* with the asymmetric unit containing one eighth of the cage and one quarter of a BF$_4^-$ counterion (**Figure 3** and **Supplementary Material**). The other BF$_4^-$ anions and some acetonitrile molecules could not be modeled sensibly thus the SQUEEZE routine was employed to account for the diffuse electron density (**Supplementary Material**). The data revealed the expected [Pd$_2$(**L$_q$**)$_4$]$^{4+}$ cage structure. The Pd-N bond lengths (Pd1-N2 2.045 Å) were similar to what have been previously observed for the related [Pd$_2$(**L$_{tripy}$**)$_4$]$^{4+}$ cages where the Pd-N bond lengths range from 2.016 to 2.027 Å (Lewis et al., 2012; Lewis and Crowley, 2014). The **L$_q$** ligands of the cage are twisted giving a V-shaped conformation where the terminal quinoline and central pyridyl heterocyclic units are not co-planar which is quite different to what was observed with the [Pd$_2$(**L$_{tripy}$**)$_4$]$^{4+}$ cages. In X-ray structures of the parent [Pd$_2$(**L$_{tripy}$**)$_4$]$^{4+}$ cages the **L$_{tripy}$** ligands were found in a linear conformation with the heterocyclic units coplanar. The twisting also alters the Pd1-Pd1$'$ distance within **C$_q$** related to the [Pd$_2$(**L$_{tripy}$**)$_4$]$^{4+}$ cages. The Pd1-Pd1$'$ distances for the parent [Pd$_2$(**L$_{tripy}$**)$_4$]$^{4+}$ cages range from 11.49 to 12.24 Å, whereas the Pd1-Pd1$'$ distance was found to be longer (12.506 Å) suggesting that the **C$_q$** cage has a larger cavity despite featuring the same 2,6-diethynylpyridine linker units. The [Pd(**quinoline**)$_4$]$^{2+}$ units at the top and bottom of **C$_q$** are twisted in opposite directions, the top cationic unit has a right handed twist while the bottom cationic unit has a left handed twist giving an overall *meso* structure (**Figures 3B,C** and **Supplementary Material**). Despite extensive efforts we were unable to obtain X-ray diffraction quality single crystals of **C$_{iq}$**. Thus, to gain further insight into the structure of **C$_{iq}$** we modeled the cage using Density Functional Theory (DFT) calculations (**Figures 3D,E**). Energy minimization of **C$_{iq}$** (DFT, BP86 def2-SVP, acetonitrile solvation, **Supplementary Material**) showed that the cage adopted a lantern shape similar to what was previously observed for [Pd$_2$(**L$_{tripy}$**)$_4$]$^{4+}$ cages (Lewis et al., 2012; Lewis and Crowley, 2014). The calculated Pd – N bond distances (2.049 Å) and the Pd-Pd$'$ distance (11.758 Å) match well with those observed crystallographically for the related [Pd$_2$(**L$_{tripy}$**)$_4$]$^{4+}$ cages. The **L$_{iq}$** ligand adopts a linear conformation with all the heterocyclic units coplanar. The DFT calculations indicated that the **C$_{iq}$** is structurally very similar to the parent [Pd$_2$(**L$_{tripy}$**)$_4$]$^{4+}$ cages whereas the **C$_q$** is more twisted and provided a cavity of different size and shape to the parent cages and the **C$_{iq}$** system.

We and others have previously shown that other similar [Pd$_2$(**L$_{tripy}$**)$_4$]$^{4+}$ cages can encapsulate cisplatin through hydrogen bonding interactions in CH$_3$CN and DMF solvents (Lewis et al., 2012, 2013, 2014; Kaiser et al., 2016; Preston et al., 2016, 2017; Schmidt et al., 2016b). Therefore, we examined the ability of **C$_{iq}$** and **C$_q$** to interact with cisplatin in CH$_3$CN using ^{1}H NMR spectroscopy. Addition of an excess of cisplatin to a
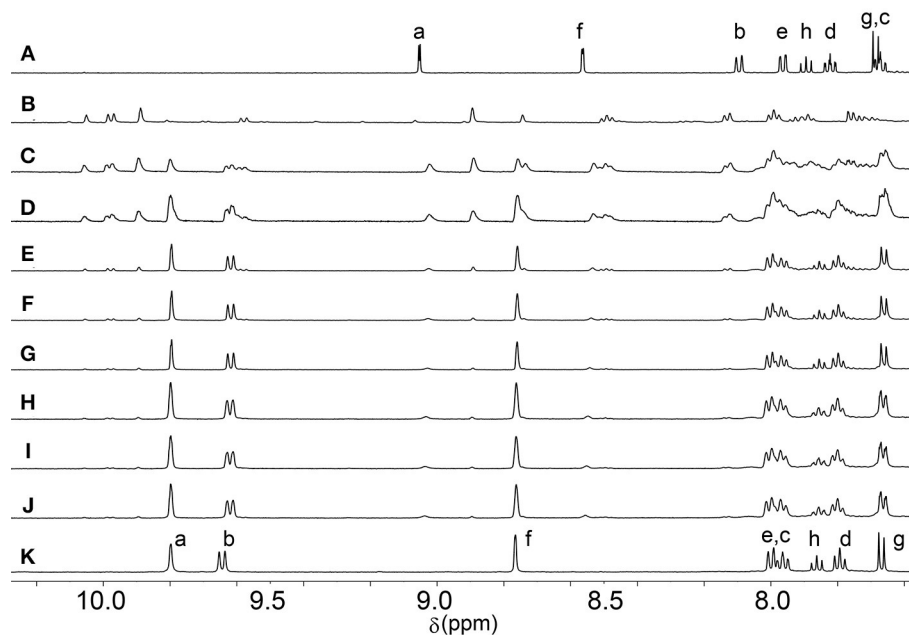
FIGURE 2 | Partial ^{1}H NMR (500 MHz, CD$_3$CN, 338 K) spectra showing the formation of **C$_q$** over time at 65°C. **(A) L$_q$**, **(B)** initial complexation ($t = 0$), **(C)** $t = 30$ min, **(D)** $t = 1$ h, **(E)** $t = 2$ h, **(F)** $t = 3$ h, **(G)** $t = 4$ h, **(H)** $t = 5$ h, **(I)** $t = 6$ h, **(J)** $t = 7$ h, **(K)** isolated **C$_q$**.

CD$_3$CN solution of the **C$_{iq}$** cage resulted in a downfield shift and broadening ($\Delta\delta = 0.03$ ppm) of the internally directed cage proton H$_a$ (**Figures 4A,B**) indicative of cisplatin binding within the cage cavity, albeit weakly. A similar ^{1}H NMR experiment was carried out with the **C$_q$** cage (**Figures 4C,D**). However, with the **C$_q$** cage no shifts were observed for any of the cage proton resonances in the presence of an excess of cisplatin suggesting that the more twisted **C$_q$** cage does not interact with the anticancer agent. The behavior was similar to what has been observed with a related twisted [Pd$_2$(**L$_{2Atripy}$**)$_4$]$^{4+}$ cage (where **L$_{2Atripy}$** = 2,6-*bis*[2-(6-amino-3-pyridinyl)ethynyl]-4-pyridinemethanol) (Preston et al., 2016). The [Pd$_2$(**L$_{2Atripy}$**)$_4$]$^{4+}$ cage did not bind cisplatin in DMF solvent and the lack of binding was ascribed to the twisted cage cavity which was not as preorganised as those of the related lantern shaped [Pd$_2$(**L$_{tripy}$**)$_4$]$^{4+}$ cages. Presumably the different sized cavity and different spatial arrangement of the hydrogen bond donors and acceptors caused by the twisting observed in the crystal structure of **C$_q$** impedes the cisplatin-**C$_q$** interaction in this case.

The kinetic robustness of the related [Pd$_2$(**L$_{tripy}$**)$_4$]$^{4+}$ architectures in the presence of common biological nucleophiles (chloride (Cl$^-$), histidine and cysteine) has been determined using ^{1}H NMR competition experiments. When the parent [Pd$_2$(**L$_{tripy}$**)$_4$]$^{4+}$ architectures were treated with 8 equivalents of tetrabutylammonium chloride the pyridyl substituted cages were rapidly and quantitatively decomposed (in <5 min). To examine the effect of substituting the pyridyl donor units for quinoline heterocycles time-course ^{1}H NMR competition experiments were carried out in d_6-DMSO where 2 mM solutions of each cage (**C$_q$** or **C$_{iq}$**) were treated with 8 equivalents of tetrabutylammonium chloride at 298 K (**Figure 5** and

Supplementary Material). Within 30 s of adding Cl$^-$ to the **C$_{iq}$** cage, there were multiple species observed in the ^{1}H NMR spectrum. These were attributed to the **C$_{iq}$** cage, [Cl⊂**C$_{iq}$**]$^{3+}$, the [Pd$_2$(**L$_{iq}$**)$_2$Cl$_4$] macrocycle and free ligand based on our own previous results (Preston et al., 2015) and related literature. After 50 min, only uncoordinated ligand was visible in the ^{1}H NMR spectrum (**Supplementary Material**).

Under the same conditions, **C$_q$** was stable for 1 h before showing signs of decomposition (**Figure 5**). After 3 h, there was no evidence of the **C$_q$** cage, and the ^{1}H NMR spectrum displayed peaks corresponding to free ligand and a second metal-containing species, which based on the observed chemical shifts was most likely the neutral [Pd$_2$(**L$_q$**)$_2$Cl$_4$] macrocycle (**Figure 5H**). This degradation behavior has been seen before with the [Pd$_2$(**L$_{tripy}$**)$_4$]$^{4+}$ system in DMF (Preston et al., 2015). After 7 h, only free ligand could observed in the ^{1}H NMR spectrum indicating that all the ligand containing metal complexes had been completely decomposed into [Pd(Cl)$_4$]$^{2-}$ (**Figure 5J**).

In comparison to the previously reported [Pd$_2$(**L$_{tripy}$**)$_4$]$^{4+}$ cage ($\tau_{1/2} = 2$ min), the isoquinoline cage displayed an identical half-life ($\tau_{1/2} = 2$ min), whereas the quinoline system was considerably more robust ($\tau_{1/2} = 2$ h). Presumably the observed results reflect the different steric profiles of the two quinoline substituted cages (**C$_q$** or **C$_{iq}$**). The **C$_q$** cage has the quinoline moieties protecting the external face of the palladium, providing more impediment to nucleophilic attack from that face (**Figure 6**). The **C$_{iq}$** does not feature the same steric impediment as the benzene units of the isoquinoline heterocycles do not block the top face of the **C$_{iq}$** cage as much as they do in the quinoline **C$_q$** (**Figure 6**).
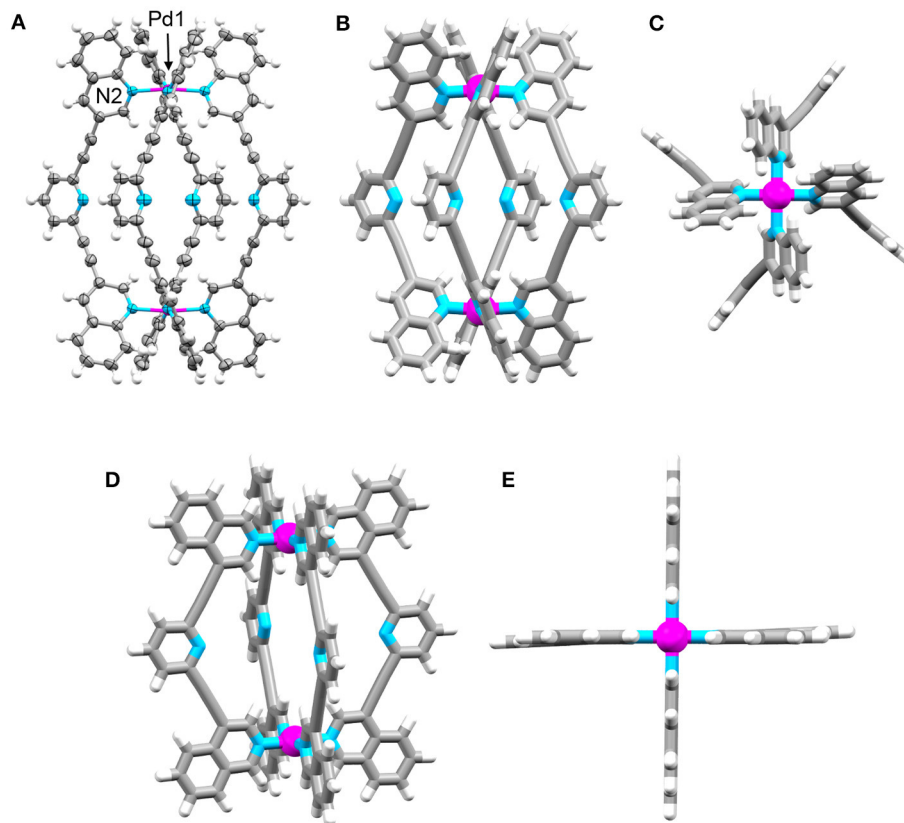
FIGURE 3 | Molecular structures of **C$_q$** and **C$_{iq}$**. X-ray structure of **C$_q$**: **(A)** ellipsoid side view, **(B)** tube side view, and **(C)** tube top view showing paddle-like array of quinoline panels over palladium(II) center. Solvent molecules and counterions have been omitted for clarity. Ellipsoids are shown at 50% probability. DFT optimized (BP86 def2-SVP) model of **C$_{iq}$**; **(D)** side view and **(E)** top view showing lantern-shaped structure. Colors: carbon gray, nitrogen blue, palladium magenta, hydrogen white.
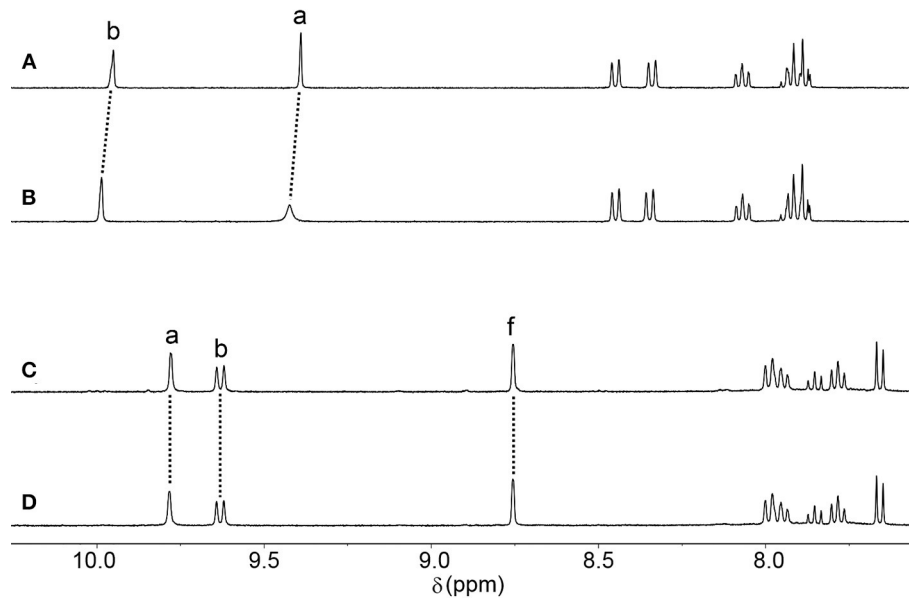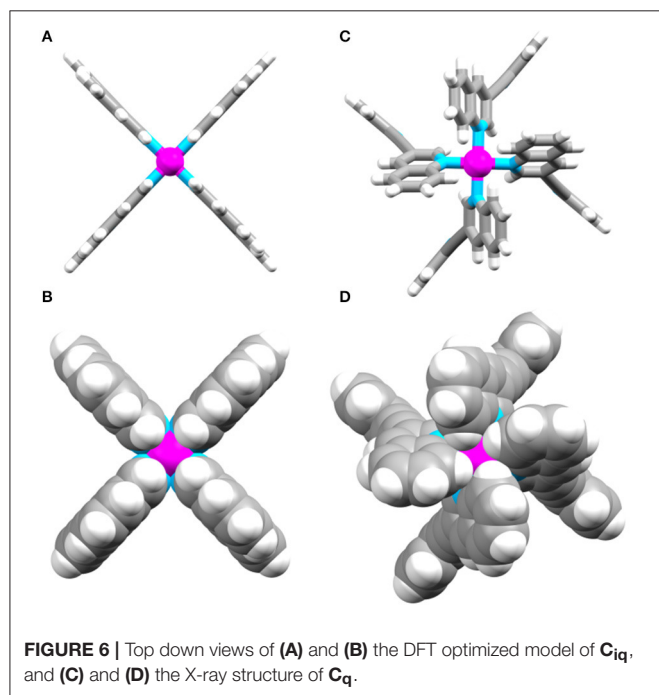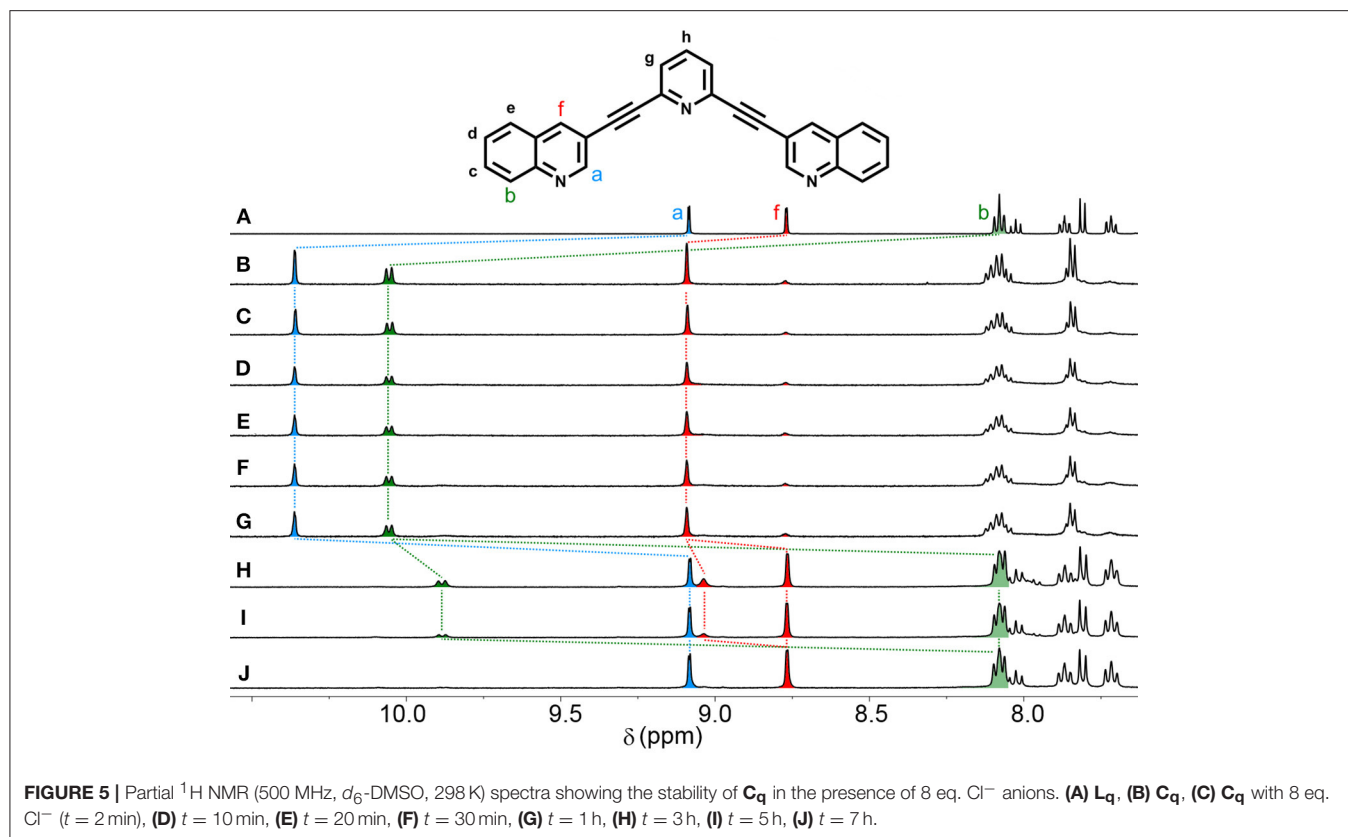

FIGURE 4 | Partial ^{1}H NMR (500 MHz, CD$_3$CN, 298 K) stacked plot of **(A) C$_{iq}$ (B) C$_{iq}$** + cisplatin (10 eq.) **(C) C$_q$**, and **(D) C$_q$** + cisplatin (10 eq.).

FIGURE 5 | Partial ^{1}H NMR (500 MHz, d_6-DMSO, 298 K) spectra showing the stability of $\mathbf{C_q}$ in the presence of 8 eq. Cl⁻ anions. **(A) $\mathbf{L_q}$, (B) $\mathbf{C_q}$, (C) $\mathbf{C_q}$** with 8 eq. Cl⁻ ($t = 2$ min), **(D)** $t = 10$ min, **(E)** $t = 20$ min, **(F)** $t = 30$ min, **(G)** $t = 1$ h, **(H)** $t = 3$ h, **(I)** $t = 5$ h, **(J)** $t = 7$ h.

FIGURE 6 | Top down views of **(A)** and **(B)** the DFT optimized model of $\mathbf{C_{iq}}$, and **(C)** and **(D)** the X-ray structure of $\mathbf{C_q}$.

To assess biological activity, the cytotoxic effect (as half-maximal inhibitory concentrations (IC$_{50}$)) of the ligands and cages were determined against three different cell lines: cisplatin resistant MDA-MB-231 (breast cancer) (Lehmann et al., 2011), A549 (lung cancer) and non-cancerous primary cells: adult human dermal fibroblasts (HDFa) (**Table 1** and **Supplementary Material**). The ligands $\mathbf{L_q}$ and $\mathbf{L_{iq}}$ exhibited limited solubility, and so data above the concentration of 1 µM was unattainable. Below this threshold, $\mathbf{L_{iq}}$ displayed minimal cytotoxic activity against both cell lines, while $\mathbf{L_q}$ was shown to be cytotoxic against A549 (IC$_{50}$ = 0.5 µM). Both cages were observed to be cytotoxic against the malignant cell lines, with $\mathbf{C_q}$ showing the same level of toxicity as its ligand against lung cancer cells (IC$_{50}$ = 0.5 µM). $\mathbf{C_q}$ was slightly less cytotoxic against MDA-MB-231 (IC$_{50}$ = 1.7 µM), whereas $\mathbf{C_{iq}}$ was less cytotoxic than the quinoline analog, with the IC$_{50}$ values ranging from 4.0 to 7.4 µM against the cancer cells. Both quinoline cages were found to be considerably more active than the related parent [Pd$_2$($\mathbf{L_{tripy}}$)$_4$]⁴⁺ cage system (IC$_{50}$ = 41.4 and 56.7 µM against A549 and MDA-MB-231, respectively) (McNeill et al., 2015). The quinoline cages were also more active than cisplatin against the two cancer lines examined (cisplatin IC$_{50}$ values = 41.2 and 9.4 µM, against MDA-MB-231 and A549, respectively) (Lo et al., 2015; McNeill et al., 2015). The quinoline cages $\mathbf{C_q}$ and $\mathbf{C_{iq}}$ were more cytotoxic than all the [Pd$_2$($\mathbf{L_{tripy}}$)$_4$]⁴⁺ cage systems reported in the literature (IC$_{50}$ values for the $\mathbf{L_{tripy}}$ based systems ranged from 10 to 100 µM) (McNeill et al., 2015; Kaiser et al., 2016; Schmidt et al., 2016b). Additionally, $\mathbf{C_q}$ was also more active, albeit against different cancer cell lines (HL-60, HL-60/Dox, HT-29, T-24, SKW-3), than the hydrophobic [Pd$_2$($\mathbf{L_{anthracene}}$)$_4$]⁴⁺ cages of Yoshizawa and Ahmedova (IC$_{50}$ values ranged from 0.9 to 37.4 µM) (Ahmedova et al., 2016; Anife et al., 2016).

TABLE 1 | Half-maximal inhibitory concentrations (IC$_{50}$) of ligands **L$_q$** and **L$_{iq}$**, and cages **C$_q$** and **C$_{iq}$** architectures at 24 h.

Compound	IC$_{50}^a$ (µM)			
	MDA-MB-231	A549	HDFa	MCF-10A^b
L$_q$	>1^c	0.5 ± 0.1	>1^c	–
C$_q$	1.7 ± 0.1	0.5 ± 0.1	2.6 ± 0.4	–
L$_{iq}$	>1^c	>1^c	>1^c	–
C$_{iq}$	4.0 ± 0.3	7.4 ± 1.0	3.0 ± 0.4	–
L$_{hextrz}$ (McNeill et al., 2015)	89.8 ± 10.7	28.5 ± 2.6	–	18.1 ± 3.1
C$_{hextrz}$ (McNeill et al., 2015)	6.0 ± 0.6	6.9 ± 0.9	–	8.1 ± 1.2
L$_{tripy}$ (McNeill et al., 2015)	>100	95.3 ± 9.7	–	>100
C$_{tripy}$ (McNeill et al., 2015)	56.7 ± 2.2	41.4 ± 3.9	–	71.4 ± 3.9
cisplatin (Lo et al., 2015; McNeill et al., 2015)	41.2 ± 3.9	9.4 ± 0.3	–	–

L$_{tripy}$, **C$_{tripy}$**, **L$_{hextrz}$**, **C$_{hextrz}$** and cisplatin (Lo et al., 2015) have been added for comparison (McNeill et al., 2015).
^{a}IC$_{50}$ values are given as mean ± SE.
^{b}The **C$_{tripy}$** and **C$_{hextrz}$** cages were tested against MCF-10A as a non-cancerous control.
^{c}Solubility limited the range of concentrations to below 1 µM. " – " = Not determined.

C$_q$ was also more cytotoxic than a hydrophobic *bis*-hexyl-1,2,3-triazole substituted [Pd$_2$(**L$_{hextrz}$**)$_4$]$^{4+}$ helicate, **C$_{hextrz}$**, we developed previously (IC$_{50}$ values = 6.9 and 6.0 µM against A549 and MDA-MB-231, respectively) (McNeill et al., 2015). We presume that the favorable combination of high hydrophobicity and the kinetic robustness against biological nucleophiles leads to the higher observed activity of **C$_q$** relative to the other [Pd$_2$(**L**)$_4$]$^{4+}$ architectures. Disappointingly, neither of the cages (**C$_q$** and **C$_{iq}$**) showed any selectivity for the cancer cells, they were all found to have similar cytotoxicity against HDFa skin cells (IC$_{50}$ values ranged from 2.6 to 3.0 µM).

CONCLUSION

We have herein reported the synthesis, characterization, cisplatin binding, kinetic robustness and cytotoxicity of two new *bis*-isoquinoline and *bis*-quinoline derived [Pd$_2$(**L**)$_4$]$^{4+}$ cage complexes. The crystal structure of **C$_q$** architecture showed that the [Pd$_2$(**L**)$_4$]$^{4+}$ cage formed a twisted *meso* isomer where the [Pd(**quinoline**)$_4$]$^{2+}$ units at either end of the cage architecture adopt the opposite twists (left and right handed). Conversely, Density Functional Theory (DFT) calculations on the **C$_{iq}$** cage architecture indicated that a lantern shaped conformation similar to what has been observed before for related [Pd$_2$(**L$_{tripy}$**)$_4$]$^{4+}$ systems was generated. The different cage conformations resulted in different properties for the isomeric cages. The **C$_{iq}$** cage is able to bind, weakly in acetonitrile, the anticancer drug cisplatin whereas the **C$_q$** architecture shows no interaction with the guest under the same conditions. The kinetic robustness of the two cages in the presence of Cl$^-$ nucleophiles was also different. The **C$_{iq}$** cage was completely decomposed into free **L$_{iq}$** and [Pd(Cl)$_4$]$^{2-}$ within 1 h. However, the **C$_q$** cage was more long lived and was only fully decomposed after 7 h. The ligands (**L$_{iq}$** and **L$_q$**) and cages (**C$_{iq}$** and **C$_q$**) were assessed for their cytotoxic properties against two cancerous cell lines (A549 lung cancer cells and MDA-MB-231 breast cancer cells) and one non-cancerous cell line (HDFa skin cells). It was found that **L$_q$** and **C$_q$** were both reasonably cytotoxic against A549, while **C$_{iq}$** was slightly

less active. The higher observed cytotoxicity of **C$_q$** relative to the other [Pd$_2$(**L**)$_4$]$^{4+}$ architectures was presumed to be due the favorable combination of high hydrophobicity and the kinetic robustness against biological nucleophiles. However, none of the new molecules showed any selectivity for cancer cells, they were all found to have similar cytotoxicity against HDFa skin cells. A range of [Pd$_2$(**L**)$_4$]$^{4+}$ cage systems have now been shown to be cytotoxic. However, in order to advance this class of MSA as anticancer agents more in depth mode of action/mechanistic studies on the origins of the cytotoxic activity are required. Studies to this effect are now underway.

AUTHOR CONTRIBUTIONS

RV and JC conceived the idea, analyzed the data and wrote the manuscript. RV and LG conducted the synthesis. RV and DP conducted stability studies. RV, DP, and JJ conducted cytotoxicity studies. GG oversaw the cytotoxicity studies and analyzed the data. All authors provided feedback on the manuscript drafts and approved the submission.

New Zealand's national facilities are provided by the New Zealand eScience Infrastructure and funded jointly by NeSI's collaborator institutions and through the Ministry of Business, Innovation and Employment's Research Infrastructure program. URL: https://www.nesi.org.

SUPPLEMENTARY MATERIAL

The Supplementary Material for this article can be found online at: https://www.frontiersin.org/articles/10.3389/fchem.2018.00563/full#supplementary-material

REFERENCES

Ahmedova, A., Mihaylova, R., Momekova, D., Shestakova, P., Stoykova, S., Zaharieva, J., et al. (2016). M2L4 coordination capsules with tunable anticancer activity upon guest encapsulation. *Dalton Trans.* 45, 13214–13221. doi: 10.1039/C6DT01801G

Allison, S. J., Cooke, D., Davidson, F. S., Elliott, P. I. P., Faulkner, R. A., Griffiths, H. B. S., et al. (2018). Ruthenium-containing linear helicates and mesocates with tuneable p53-selective cytotoxicity in colorectal cancer cells. *Angew. Chem. Int. Ed.* 57, 9799–9804. doi: 10.1002/anie.201805510

Anife, A., Denitsa, M., Masahiro, Y., Pavletta, S., Georgi, M., Munetaka, A., et al. (2016). Anticancer potencies of PtII- and PdII-linked M₂L₄ coordination capsules with improved selectivity. *Chem. Asian J.* 11, 474–477. doi: 10.1002/asia.201501238

Bhat, I. A., Jain, R., Siddiqui, M. M., Saini, D. K., and Mukherjee, P. S. (2017). Water-soluble Pd₈L₄ self-assembled molecular barrel as an aqueous carrier for Hydrophobic Curcumin. *Inorg. Chem.* 56, 5352–5360. doi: 10.1021/acs.inorgchem.7b00449

Bloch, W. M., Abe, Y., Holstein, J. J., Wandtke, C. M., Dittrich, B., and Clever, G. H. (2016). Geometric complementarity in assembly and guest recognition of a bent Heteroleptic cis-[Pd₂LA₂LB₂] coordination cage. *J. Am. Chem. Soc.* 138, 13750–13755. doi: 10.1021/jacs.6b08694

Bloch, W. M., Holstein, J. J., Hiller, W., and Clever, G. H. (2017). Morphological control of Heteroleptic cis- and trans-Pd₂L₂L′₂ cages. *Angew. Chem. Int. Ed.* 56, 8285–8289. doi: 10.1002/anie.201702573

Bondy, C. R., Gale, P. A., and Loeb, S. J. (2004). Metal-organic anion receptors: arranging urea hydrogen-bond donors to encapsulate sulfate ions. *J. Am. Chem. Soc.* 126, 5030–5031. doi: 10.1021/ja039712q

Casini, A., Woods, B., and Wenzel, M. (2017). The Promise of Self-Assembled 3D Supramolecular coordination complexes for biomedical applications. *Inorg. Chem.* 56, 14715–14729. doi: 10.1021/acs.inorgchem.7b02599

Cook, T. R., and Stang, P. J. (2015). Recent developments in the preparation and chemistry of metallacycles and metallacages via coordination. *Chem. Rev.* 115, 7001–7045. doi: 10.1021/cr5005666

Cook, T. R., Vajpayee, V., Lee, M. H., Stang, P. J., and Chi, K.-W. (2013). Biomedical and biochemical applications of self-assembled metallacycles and metallacages. *Acc. Chem. Res.* 46, 2464–2474. doi: 10.1021/ar400010v

Dubey, A., Jeong, Y. J., Jo, J. H., Woo, S., Kim, D. H., Kim, H., et al. (2015). Anticancer activity and autophagy involvement of self-assembled arene-ruthenium metallacycles. *Organometallics* 34, 4507–4514. doi: 10.1021/acs.organomet.5b00512

Faulkner, A. D., Kaner, R. A., Abdallah, Q. M., Clarkson, G., Fox, D. J., Gurnani, P., et al. (2014). Asymmetric triplex metallohelices with high and selective activity against cancer cells. *Nat. Chem.* 6, 797–803. doi: 10.1038/nchem.2024

Garci, A., Castor, K. J., Fakhoury, J., Do, J.-L., Di Trani, J., Chidchob, P., et al. (2017). Efficient and rapid mechanochemical assembly of Platinum(II) squares for guanine quadruplex targeting. *J. Am. Chem. Soc.* 139, 16913–16922. doi: 10.1021/jacs.7b09819

Grishagin, I. V., Kushal, S., Olenyuk, B. Z., Pollock, J. B., Cook, T. R., and Stang, P. J. (2014). *In vivo* anticancer activity of rhomboidal Pt(II) metallacycles. *Proc. Natl. Acad. Sci. U.S.A.* 111, 18448–18453. doi: 10.1073/pnas.1418712111

Han, J., Schmidt, A., Zhang, T., Permentier, H., Groothuis, G. M., Bischoff, R., et al. (2017). Bioconjugation strategies to couple supramolecular exo-functionalized palladium cages to peptides for biomedical applications. *Chem. Commun.* 53, 1405–1408. doi: 10.1039/C6CC08937B

Hotze, A. C. G., Hodges, N. J., Hayden, R. E., Sanchez-Cano, C., Paines, C., Male, N., et al. (2008). Supramolecular iron cylinder with unprecedented DNA binding is a potent cytostatic and apoptotic agent without exhibiting genotoxicity. *Chem. Biol.* 15, 1258–1267. doi: 10.1016/j.chembiol.2008.10.016

Howson, S. E., Bolhuis, A., Brabec, V., Clarkson, G. J., Malina, J., Rodger, A., et al. (2012). Optically pure, water-stable metallo-helical 'flexicate' assemblies with antibiotic activity. *Nat. Chem.* 4, 31–36. doi: 10.1038/nchem.1206

Kaiser, F., Schmidt, A., Heydenreuter, W., Altmann, P. J., Casini, A., Sieber, S. A., et al. (2016). Self-assembled palladium and platinum coordination cages: photophysical studies and anticancer activity. *Eur. J. Inorg. Chem.* 2016, 5189–5196. doi: 10.1002/ejic.201600811

Kim, T. Y., Lucas, N. T., and Crowley, J. D. (2015). A diaryl-linked [Pd₂L₄]4+ metallosupramolecular architecture: synthesis, structures and cisplatin binding studies. *Supramol. Chem.* 27, 734–745. doi: 10.1080/10610278.2015.1063633

Lehmann, B. D., Bauer, J. A., Chen, X., Sanders, M. E., Chakravarthy, A. B., Shyr, Y., et al. (2011). Identification of human triple-negative breast cancer subtypes and preclinical models for selection of targeted therapies. *J. Clin. Invest.* 121, 2750–2767. doi: 10.1172/JCI45014

Lewis, J. E., McAdam, C. J., Gardiner, M. G., and Crowley, J. D. (2013). A facile "click" approach to functionalised metallosupramolecular architectures. *Chem. Commun.* 49, 3398–3400. doi: 10.1039/c3cc41209a

Lewis, J. E. M., and Crowley, J. D. (2014). Exo- and endo-hedral interactions of counteranions with tetracationic Pd₂L₄ metallosupramolecular architectures. *Supramol. Chem.* 26, 173–181. doi: 10.1080/10610278.2013.842644

Lewis, J. E. M., Elliott, A. B. S., McAdam, C. J., Gordon, K. C., and Crowley, J. D. (2014). 'Click' to functionalise: synthesis, characterisation and enhancement of the physical properties of a series of exo- and endo-functionalised Pd₂L₄ nanocages. *Chem. Sci.* 5, 1833–1843. doi: 10.1039/c4sc00434e

Lewis, J. E. M., Gavey, E. L., Cameron, S. A., and Crowley, J. D. (2012). Stimuli-responsive Pd₂L₄ metallosupramolecular cages: towards targeted cisplatin drug delivery. *Chem. Sci.* 3, 778–784. doi: 10.1039/c2sc00899h

Li, M., Howson, S. E., Dong, K., Gao, N., Ren, J., Scott, P., et al. (2014). Chiral metallohelical complexes enantioselectively target Amyloid β for treating Alzheimer's disease. *J. Am. Chem. Soc.* 136, 11655–11663. doi: 10.1021/ja502789e

Lo, W. K., Huff, G. S., Preston, D., McMorran, D. A., Giles, G. I., Gordon, K. C., et al. (2015). A dinuclear Platinum(II) N4Py complex: an unexpected coordination mode for N4Py. *Inorg. Chem.* 54, 6671–6673. doi: 10.1021/acs.inorgchem.5b01032

Mal, P., Breiner, B., Rissanen, K., and Nitschke, J. R. (2009). White Phosphorus is air-stable within a self-assembled tetrahedral capsule. *Science* 324, 1697–1699. doi: 10.1126/science.1175313

Malina, J., Scott, P., and Brabec, V. (2015). Recognition of DNA/RNA bulges by antimicrobial and antitumor metallohelices. *Dalton Trans.* 44, 14656–14665. doi: 10.1039/C5DT02018B

Martí-Centelles, V., Lawrence, A. L., and Lusby, P. J. (2018). High activity and efficient turnover by a simple, self-assembled "Artificial Diels-Alderase". *J. Am. Chem. Soc.* 140, 2862–2868. doi: 10.1021/jacs.7b12146

McMorran, D. A., and Steel, P. J. (1998). The first coordinatively saturated, quadruply stranded helicate and its encapsulation of a hexafluorophosphate anion. *Angew Chem. Int. Ed.* 37, 3295–3297.

McNeill, S. M., Preston, D., Lewis, J. E., Robert, A., Knerr-Rupp, K., Graham, D. O., et al. (2015). Biologically active [Pd₂L₄]⁴⁺ quadruply-stranded helicates: stability and cytotoxicity. *Dalton Trans.* 44, 11129–11136. doi: 10.1039/C5DT01259G

Mitchell, D. E., Clarkson, G., Fox, D. J., Vipond, R. A., Scott, P., and Gibson, M. I. (2017). Antifreeze protein mimetic metallohelices with potent ice recrystallization inhibition activity. *J. Am. Chem. Soc.* 139, 9835–9838. doi: 10.1021/jacs.7b05822

Mjos, K. D., and Orvig, C. (2014). Metallodrugs in medicinal inorganic chemistry. *Chem. Rev.* 114, 4540–4563. doi: 10.1021/cr400460s

Oleksy, A., Blanco, A. G., Boer, R., Usón, I., Aymamí, J., Rodger, A., et al. (2006). Molecular recognition of a three-way DNA junction by a Metallosupramolecular helicate. *Angew. Chem. Int. Ed.* 45, 1227–1231. doi: 10.1002/anie.200503822

Phongtongpasuk, S., Paulus, S., Schnabl, J., Sigel, R. K., Spingler, B., Hannon, M. J., et al. (2013). Binding of a designed anti-cancer drug to the central cavity of an RNA three-way junction. *Angew. Chem. Int. Ed.* 52, 11513–11516. doi: 10.1002/anie.201305079

Preston, D., Fox-Charles, A., Lo, W. K. C., and Crowley, J. D. (2015). Chloride triggered reversible switching from a metallosupramolecular [Pd2L4]$^{4+}$ cage to a [Pd2L2Cl4] metallo-macrocycle with release of endo- and exo-hedrally bound guests. *Chem. Commun.* 51, 9042–9045. doi: 10.1039/C5CC02226F

Preston, D., Lewis, J. E., and Crowley, J. D. (2017). Multicavity [Pd$_n$L4]$^{2n+}$ cages with controlled segregated binding of different guests. *J. Am. Chem. Soc.* 139, 2379–2386. doi: 10.1021/jacs.6b11982

Preston, D., McNeill, S. M., Lewis, J. E., Giles, G. I., and Crowley, J. D. (2016). Enhanced kinetic stability of [Pd2L4]$^{4+}$ cages through ligand substitution. *Dalton Trans.* 45, 8050–8060. doi: 10.1039/C6DT00133E

Richards, A. D., Rodger, A., Hannon, M. J., and Bolhuis, A. (2009). Antimicrobial activity of an iron triple helicate. *Int. J. Antimicrob. Agents* 33, 469–472. doi: 10.1016/j.ijantimicag.2008.10.031

Samanta, S. K., Moncelet, D., Briken, V., and Isaacs, L. (2016). Metal-organic Polyhedron capped with Cucurbit[8]uril delivers Doxorubicin to cancer cells. *J. Am. Chem. Soc.* 138, 14488–14496. doi: 10.1021/jacs.6b09504

Samanta, S. K., Quigley, J., Vinciguerra, B., Briken, V., and Isaacs, L. (2017). Cucurbit[7]uril enables multi-stimuli-responsive release from the self-assembled Hydrophobic phase of a metal organic Polyhedron. *J. Am. Chem. Soc.* 139, 9066–9074. doi: 10.1021/jacs.7b05154

Schmidt, A., Casini, A., and Kuehn, F. E. (2014). Self-assembled M2L4 coordination cages: synthesis and potential applications. *Coord. Chem. Rev.* 275, 19–36. doi: 10.1016/j.ccr.2014.03.037

Schmidt, A., Hollering, M., Han, J., Casini, A., and Kühn, F. E. (2016a). Self-assembly of highly luminescent heteronuclear coordination cages. *Dalton Trans.* 45, 12297–12300. doi: 10.1039/C6DT02708C

Schmidt, A., Molano, V., Hollering, M., Pöthig, A., Casini, A., and Kühn, F. E. (2016b). Evaluation of new palladium cages as potential delivery systems for the anticancer drug Cisplatin. *Chem. Eur. J.* 22, 2253–2256. doi: 10.1002/chem.201504930

Schmitt, F., Freudenreich, J., Barry, N. P., Juillerat-Jeanneret, L., Süss-Fink, G., and Therrien, B. (2012). Organometallic cages as vehicles for intracellular release of Photosensitizers. *J. Am. Chem. Soc.* 134, 754–757. doi: 10.1021/ja207784t

Therrien, B. (2015). Biologically relevant arene ruthenium metalla-assemblies. *CrystEngComm* 17, 484–491. doi: 10.1039/C4CE02146K

Therrien, B., Suess-Fink, G., Govindaswamy, P., Renfrew, A. K., and Dyson, P. J. (2008). The "complex-in-a-complex" cations [(acac)2M⊂Ru6-(piPrC6H4Me)6(tpt)2(dhbq)3]$^{6+}$: a trojan horse for cancer cells. *Angew. Chem. Int. Ed.* 47, 3773–3776. doi: 10.1002/anie.200800186

Wang, H., Qian, X., Wang, K., Su, M., Haoyang, W.-W., Jiang, X., et al. (2018). Supramolecular Kandinsky circles with high

antibacterial activity. *Nat. Commun.* 9:1815. doi: 10.1038/s41467-018-04247-z

Wang, J.-F., Huang, L.-Y., Bu, J.-H., Li, S.-Y., Qin, S., Xu, Y.-W., et al. (2018). A fluorescent calixarene-based dimeric capsule constructed via a M(II)-terpyridine interaction: cage structure, inclusion properties and drug release. *RSC Adv.* 8, 22530–22535. doi: 10.1039/C8RA02146E

Wang, M., Vajpayee, V., Shanmugaraju, S., Zheng, Y.-R., Zhao, Z., Kim, H., et al. (2011). Coordination-driven self-assembly of M3L2 trigonal cages from preorganized metalloligands incorporating octahedral metal centers and fluorescent detection of nitroaromatics. *Inorg. Chem.* 50, 1506–1512. doi: 10.1021/ic1020719

Xu, W.-Q., Fan, Y.-Z., Wang, H.-P., Teng, J., Li, Y.-H., Chen, C.-X., et al. (2017). Investigation of binding behavior between drug molecule 5-Fluoracil and M4L4-type Tetrahedral cages: selectivity, capture, and release. *Chem. Eur. J.* 23, 3542–3547. doi: 10.1002/chem.201606060

Yi, J. W., Barry, N. P., Furrer, M. A., Zava, O., Dyson, P. J., Therrien, B., et al. (2012). Delivery of Floxuridine derivatives to cancer cells by water-soluble organometallic cages. *Bioconjugate Chem.* 23, 461–471. doi: 10.1021/bc200472n

Yoshizawa, M., and Fujita, M. (2010). Development of unique chemical phenomena within nanometer-sized, self-assembled coordination hosts. *Bull. Chem. Soc. Jpn.* 83, 609–618. doi: 10.1246/bcsj.20100035

Yoshizawa, M., Klosterman, J. K., and Fujita, M. (2009). Functional molecular flasks: new properties and reactions within discrete, self-assembled hosts. *Angew. Chem. Int. Ed.* 48, 3418–3438. doi: 10.1002/anie.200805340

Yue, Z., Wang, H., Li, Y., Qin, Y., Xu, L., Bowers, D. J., et al. (2018). Coordination-driven self-assembly of a Pt(IV) prodrug-conjugated supramolecular hexagon. *Chem. Commun.* 54, 731–734. doi: 10.1039/C7CC07622C

Zhao, A., Howson, S. E., Zhao, C., Ren, J., Scott, P., Wang, C., et al. (2017). Chiral metallohelices enantioselectively target hybrid human telomeric G-quadruplex DNA. *Nucleic Acids Res.* 45, 5026–5035. doi: 10.1093/nar/gkx244

Zheng, Y.-R., Suntharalingam, K., Bruno, P. M., Lin, W., Wang, W., Hemann, M. T., et al. (2016). Mechanistic studies of the anticancer activity of an octahedral hexanuclear Pt(II) cage. *Inorg. Chim. Acta* 452, 125–129. doi: 10.1016/j.ica.2016.03.021

Zheng, Y.-R., Suntharalingam, K., Johnstone, T. C., and Lippard, S. J. (2015). Encapsulation of Pt(IV) prodrugs within a Pt(II) cage for drug delivery. *Chem. Sci.* 6, 1189–1193. doi: 10.1039/C4SC01892C

Zhou, J., Yu, G., and Huang, F. (2017). Supramolecular chemotherapy based on host-guest molecular recognition: a novel strategy in the battle against cancer with a bright future. *Chem. Soc. Rev.* 46, 7021–7053. doi: 10.1039/C6CS00898D